

## Experimental section

### 1. Synthesis of Ni(OH)<sub>2</sub>/NF

In a typical synthesis, nickel foam (NF, 2.0cm×5.0cm) was cleaned ultrasonically by H<sub>2</sub>SO<sub>4</sub> solution (0.5M), acetone and ethanol for 30 min each, then dried at 60°C vacuum. Next, 4mmol Ni(NO<sub>3</sub>)<sub>3</sub>·6H<sub>2</sub>O, 8mmol NH<sub>4</sub>F and 20mmol urea ((NH<sub>2</sub>)<sub>2</sub>CO) were dissolved in 80mL of deionized water (DI water). Cleaned Ni foam (2.0cm×5.0cm) and the precursor solution were placed into a 100mL autoclave. The autoclave was heated at 120°C for 6h. After cooled to room temperature, the substrate was washed three times with water and ethanol, respectively, which was acquired Ni(OH)<sub>2</sub>/NF.

### 2. Synthesis of Ni<sub>3</sub>S<sub>2</sub>/NF

The as-prepared Ni(OH)<sub>2</sub>/NF was placed into a 80mL aqueous solution containing 16mmol Na<sub>2</sub>S·9H<sub>2</sub>O and heated in a 100 mL autoclave at 100°C for 8h, yielding the sample labeled as Ni<sub>3</sub>S<sub>2</sub>/NF. After being cooled, the obtained sample was washed by DI water and anhydrous ethanol, and then dried at 65°C overnight.

### 3. Synthesis of S<sub>v</sub>-Ni<sub>3</sub>S<sub>2-x</sub>P<sub>x</sub>/NF

To obtain the P doping samples, the Ni<sub>3</sub>S<sub>2</sub>/NF were placed in the tubular PECVD system (PECVD, OTF-1200X-50-4CLV-PE) under a base and treatment pressure of 0.5 Torr and heated at the rate of 10°C min<sup>-1</sup> in Ar flow of 50 sccm. The 0.3g phosphorus sources (NaH<sub>2</sub>PO<sub>2</sub>)

---

and Ni<sub>3</sub>S<sub>2</sub>/NF were put in the upstream and downstream side of the tube furnace, respectively. When heated to 300°C, the samples were treated with Ar plasma under the PH<sub>3</sub> atmosphere at 300W for 1, 2, 4, and 8 min (called Ni<sub>3</sub>S<sub>2-x</sub>P<sub>x</sub>-1/NF, Ni<sub>3</sub>S<sub>2-x</sub>P<sub>x</sub>-2/NF, Ni<sub>3</sub>S<sub>2-x</sub>P<sub>x</sub>-4/NF, and Ni<sub>3</sub>S<sub>2-x</sub>P<sub>x</sub>-8/NF), respectively.

### **Electrochemical measurements**

Electrochemical measures were performed in a CHI 660B electrochemical workstation using a standard three-electrode glass cell in 1M KOH solution. A Hg/HgO (1 mol/L KOH) served as the reference electrode, and 1cm×1cm samples were used as the working electrode. A carbon rod was used as the counter electrode to replace Pt, which may redeposit in the working electrode under testing and impact the reported results. The working electrode was activated by backward sweep method for several times to make the signal stable. The linear sweep voltammetry (LSV) curves of OER and HER were recorded by scanning potential from 0 to 0.7V and 0 to -0.3V (vs. Hg/HgO) at a scan rate of 2 mV/s and with iR compensation, respectively. All measured potentials (vs Hg/HgO) were converted to vs. RHE on the basis of the equation:  $E(\text{RHE}) = E(\text{Hg/HgO}) + 0.245\text{V} + 0.059\text{pH}$ . When the current density is  $j$ , the corresponding overpotential ( $\eta$ ) of OER is followed by the equation:  $\eta_j = E_j(\text{RHE}) - 1.23\text{ V}$ . The electrochemically active surface areas

---

(ECSAs) of the OER and HER were derived by performing CV measurements in a potential window of 0.025-0.125 V and 1.03-1.13 V vs. RHE at different scan rates of 5, 10, 20, 30, 40, and 50 mV s<sup>-1</sup>. Electrochemical impedance spectroscopy (EIS) was performed at a frequency range of 10<sup>5</sup> Hz to 0.01 Hz at a potential of the current density of 10 mA/cm<sup>-2</sup> without iR drops. The stability test was performed using the multistep method.

### **Characterization**

X-ray powder diffraction (XRD) analysis with Cu K $\alpha$  radiation was done on X'PERT (Panalytical). The Raman spectrum was performed on a Renishaw inVia system with a laser wavelength of 514nm. The chemical composition of the sample was examined by X-ray photoelectron spectroscopy (XPS, Thermo Fisher Scientific ESCALAB 250 Xi, Al K $\alpha$  radiation). The distribution and morphology were observed using scanning electron microscopy (SEM, Merlin Compact) and transmission electron microscopy (TEM, Talos).

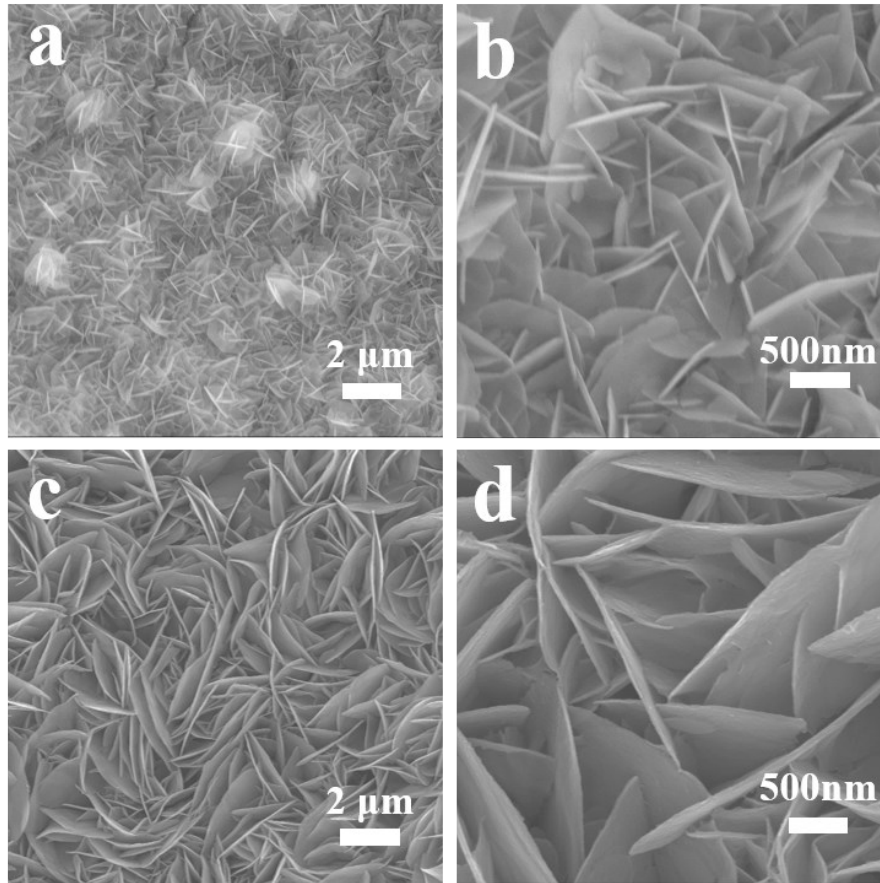


Figure S1. (a-b) SEM images of  $\text{Ni(OH)}_2/\text{NF}$ , and (c-d)  $\text{Ni}_3\text{S}_2/\text{NF}$  at different magnification.

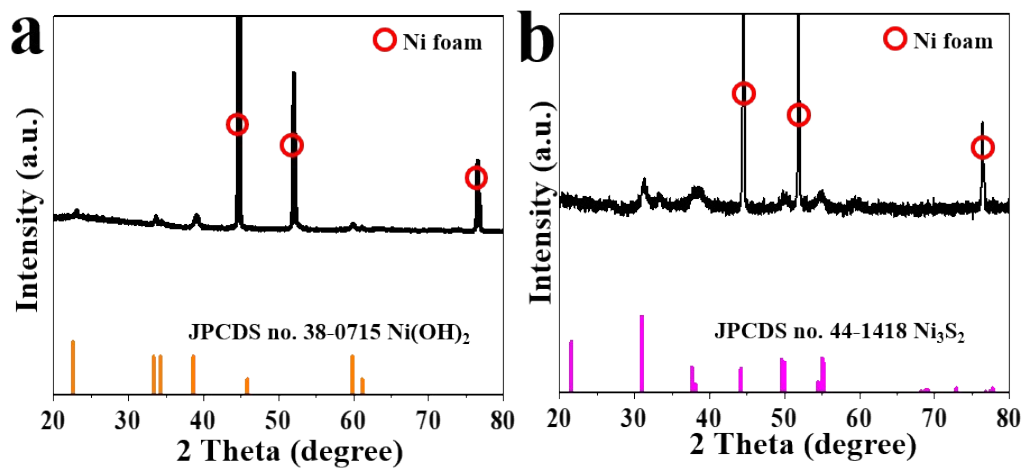


Figure S2. XRD patterns of (a)  $\text{Ni(OH)}_2/\text{NF}$ , and (b)  $\text{Ni}_3\text{S}_2/\text{NF}$ .

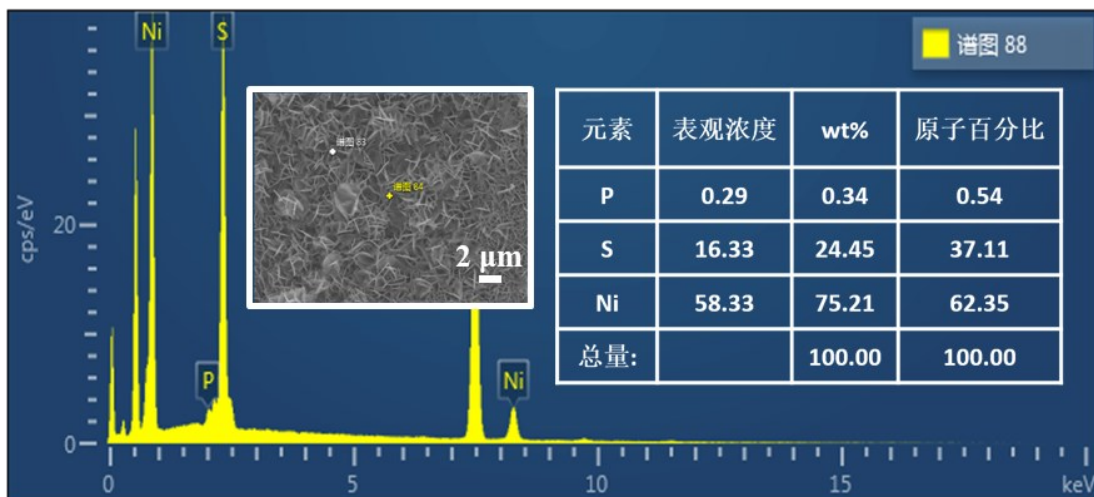


Figure S3. Energy-dispersive X-ray spectroscopy (EDX) of  $\text{Ni}_3\text{S}_{2-x}\text{P}_x/\text{NF}$ .

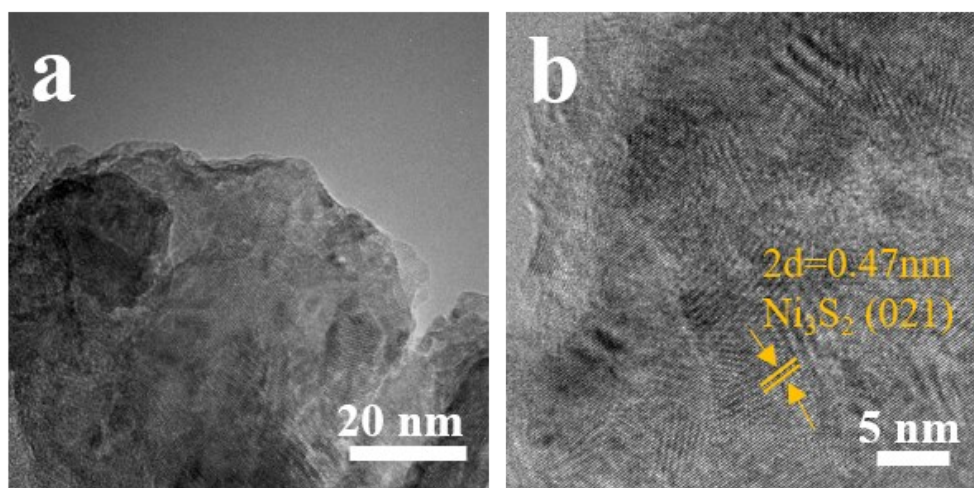


Figure S4. HRTEM images of  $\text{Ni}_3\text{S}_2/\text{NF}$ .

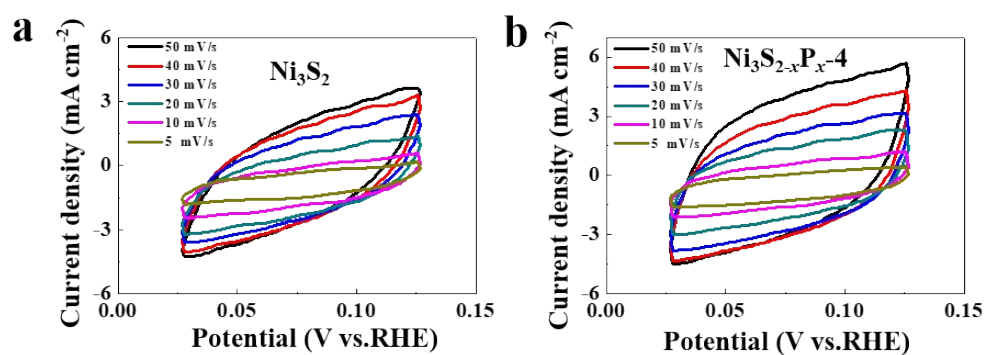


Figure S5. CV curves at different scan rates for (a)  $\text{Ni}_3\text{S}_2/\text{NF}$  and (b)  $\text{Ni}_3\text{S}_{2-x}\text{P}_x-4/\text{NF}$ . (c) Capacitive  $i = i_a - i_c$  at the potential of 0.075 V vs. RHE plotted against scan rate fitted to estimate the electrochemical double-layer capacitances ( $C_{dl}$ ).

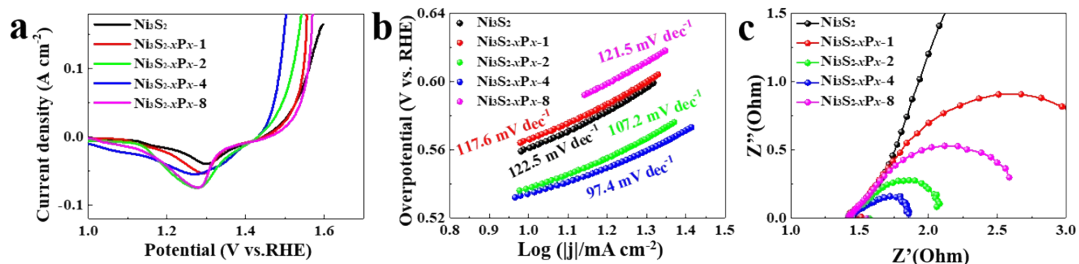


Figure S6. Electrochemical OER performance in 1 M KOH; (d) LSV curves, (e) the corresponding Tafel plots, and (f) Nyquist plots for  $\text{Ni}_3\text{S}_2/\text{NF}$  and  $\text{Ni}_3\text{S}_{2-x}\text{P}_x/\text{NF}$ .

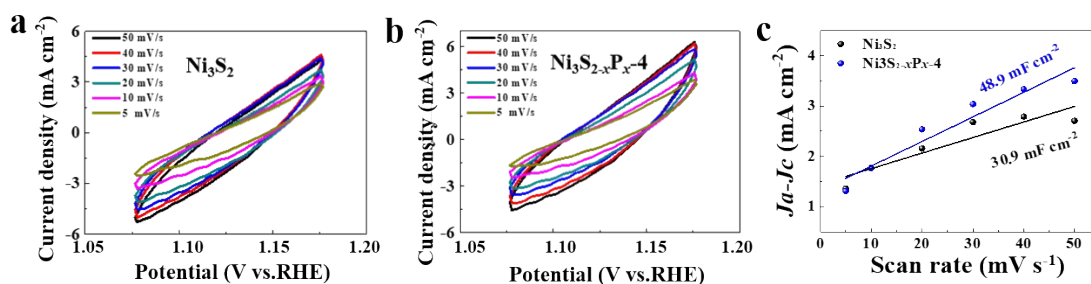


Figure S7. CV curves at different scan rates for (a)  $\text{Ni}_3\text{S}_2/\text{NF}$  and (b)  $\text{Ni}_3\text{S}_{2-x}\text{P}_x-4/\text{NF}$ . (c) Capacitive  $i = i_a - i_c$  at the potential of 1.125 V vs. RHE plotted against scan rate fitted to estimate the electrochemical double-layer capacitances ( $C_{dl}$ ).

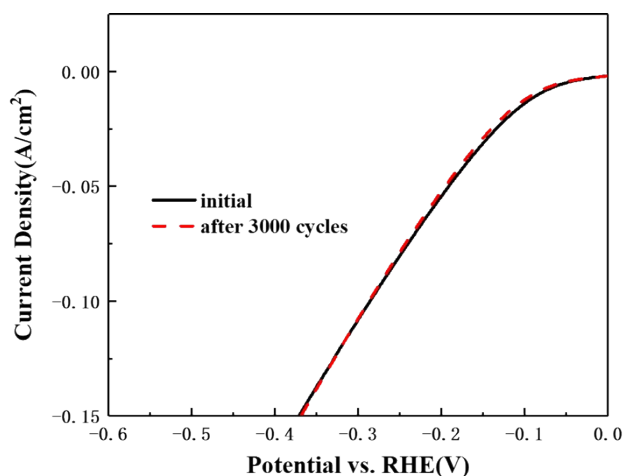


Figure S8. Comparison of the LSV curves obtained on the  $\text{Ni}_3\text{S}_{2-x}\text{P}_x-4/\text{NF}$  before and after 3000 cycles of CV potential sweep.

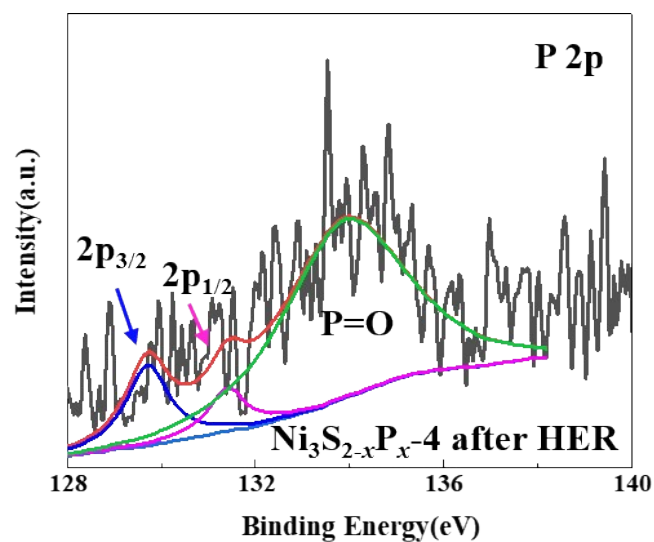


Figure S9. Fitted P 2p XPS spectra of  $\text{Ni}_3\text{S}_{2-x}\text{P}_x-4/\text{NF}$  after long-time stability test.